Earth and Planetary Science Letters 619 (2023) 118289

Contents lists available at ScienceDirect

Earth and Planetary Science Letters

journal homepage: www.elsevier.com/locate/epsl

Boron isotopes in Central American volcanics indicate a key role for the subducting oceanic crust

Stephen J. Turner [a,*,1], Mattison H. Barickman [b,c,1], Julian Rodriguez [b], David A. Fike [b,c], Clive M. Jones [b], Kun Wang [b,c], Ivan P. Savov [d,e], Samuele Agostini [e], Michael J. Krawczynski [b,c], Rita Parai [b,c]

[a] Department of Geosciences, University of Massachusetts, Amherst, MA, 01035, USA
[b] Department of Earth, Environmental, and Planetary Sciences, Washington University in St. Louis, St. Louis, MO, 63130, USA
[c] McDonnell Center for the Space Sciences, Washington University in St. Louis, St. Louis, MO 63130, USA
[d] School of Earth and Environment, University of Leeds, Leeds, UK
[e] Istituto di Geoscienze e Georisorse, Area della Ricerca di Pisa, Consiglio Nazionale delle Ricerche, I-56124, Pisa, Italy

ARTICLE INFO

Article history:
Received 6 September 2022
Received in revised form 19 May 2023
Accepted 26 June 2023
Available online 27 July 2023
Editor: R. Dasgupta

Keywords:
boron isotope
subduction
volcanic arc
Central America

ABSTRACT

The geochemistry of arc magmas can shed light on chemical outfluxes from subducting slabs to the overlying mantle. Boron (B) abundances and isotope ratios are valuable tracers of slab-derived components due to the distinct compositions of the mantle and subducting materials and distinctive isotopic fractionation during dehydration. New Be/B and δ^{11}B measurements in olivine-hosted melt inclusions (MIs) from three Nicaraguan volcanic centers (Telica, Cerro Negro, and Masaya) are consistent with a B-rich slab component that has δ^{11}B ranging from +2.9‰ to +5.9‰, slightly higher than new measurements of hemipelagic (δ^{11}B = +0.7‰±0.03 and +2.1‰±0.08; 1σ n = 3) and carbonate (δ^{11}B = +2.9‰±0.06 and 3.7±0.09; 1σ n = 3) sediments sampled by DSDP Hole 495 on the Cocos plate.
A thermochemical model of the Nicaraguan subduction zone is used to quantitatively model B loss and isotopic fractionation during slab dehydration and melting. In contrast to previous studies regarding B systematics in Central America and elsewhere, this model reproduces the range of δ^{11}B preserved in Nicaraguan olivine-hosted MIs without the involvement of serpentinite-derived fluids. The model indicates that Nicaraguan MI δ^{11}B signatures are primarily controlled by input from subducted altered oceanic crust (AOC), with a minor contribution from subducted sediments. This finding implies that the volatile element budget delivered from the slab to the volcanic arc is also mostly derived from the ocean crust, and that volatiles carried in deeper layers of the slab may be recycled beyond the arc into the deeper mantle beneath Central America.

1. Introduction

The compositions of arc lavas reflect melting of a mantle source modified by contributions from the subducting slab and provide constraints on chemical transfer between Earth's surface and interior during subduction. Water and other volatile components are mainly carried by hydrous minerals in subducting slabs. Fluids are released from the slab when these hydrous minerals metamorphically break down, and the resulting flux of volatiles causes melting in the overlying mantle wedge. Several aspects of volatile cycling in the solid Earth system remain poorly understood, however, such as the detailed sources of slab-derived fluids and hydrous melts in the slab (Cooper et al., 2020; Tonarini et al., 2011) and the impact of shear heating on dehydration reactions (van Keken et al., 2018).

Boron (B) provides a unique tool to investigate these questions. Subducting sediments, altered oceanic crust (AOC), and serpentinized lithospheric mantle are enriched in B by up to four orders of magnitude relative to the upper mantle (Bonatti et al., 1984; Spivack and Edmond, 1987; Ishikawa and Nakamura, 1993; Leeman and Sisson, 1996; Scambelluri et al., 2004; Savov et al., 2007; Scambelluri and Tonarini, 2012) and have distinct ratios of ^{10}B to ^{11}B (De Hoog and Savov, 2018; Marschall, 2018). B is partitioned preferentially into the liquid phase during either slab dehydration or melting (Kessel et al., 2005), and a temperature-dependent isotopic fractionation occurs between liquids and solids (Peacock and Hervig, 1999; Wunder et al., 2005). As a result, arc

* Corresponding author.
E-mail address: stephenjudsonturner@gmail.com (S.J. Turner).
[1] Joint first author.

https://doi.org/10.1016/j.epsl.2023.118289
0012-821X/

magma B concentrations and isotope ratios ($^{11}B/^{10}B$, expressed in per mil deviation from the standard NIST SRM 951, where $\delta^{11}B = ((^{11}B/^{10}B)_{sample}/(^{11}B/^{10}B)_{SRM\ 951} - 1) \times 1000$) can provide information about where in the slab dehydration reactions occur and at what temperature, though the details of this process are complicated by the many variables in play (De Hoog and Savov, 2018).

Prior studies of $\delta^{11}B$ in arcs have suggested that this isotope system provides evidence for geologic processes not required by other trace element and radiogenic isotope systematics. Most global and regional variations in arc-front trace element abundances and radiogenic isotopes can be understood in a framework in which ambient mantle of varying composition is transported beneath the arc front via corner flow, where it mixes with hydrous slab-derived components and melts to varying degrees (Turner and Langmuir, 2022a,b,c). These melts then differentiate in the crust and sometimes assimilate crustal material. The influence of the slab components diminishes with distance behind the arc front, leading to lower extents of melting that correlate with lower source water content (Ancellin et al., 2017; Churikova et al., 2007; Nakamura et al., 1985; Wieser et al., 2019). Within individual arcs, the $\delta^{11}B$ of erupted volcanics also decrease behind the arc front (e.g., Ishikawa and Tera, 1997). These across-arc $\delta^{11}B$ trends may reflect mixing between regionally uniform slab components and the ambient mantle wedge (Ishikawa and Tera, 1997; Iveson et al., 2021), though it has also been proposed that this trend arises due to progressive dehydration of the slab. In the latter case, the slab component delivered to rear-arc volcanoes would be compositionally distinct from the arc-front slab component (Rosner et al., 2003; Ryan et al., 1995; Leeman and Sisson, 1996; Konrad-Schmolke et al., 2016). Other studies have suggested that B isotope systematics provide geochemical evidence for tectonic erosion of forearc serpentinite (Leeman et al., 2017; Savov et al., 2007; Tonarini et al., 2011, 2007), a large fluid flux from serpentinized lithospheric mantle in the subducting plate (Cooper et al., 2020), and extensive slab dehydration beneath the forearc (Leeman et al., 2004; Walowski et al., 2016). These processes are not generally required by most regional geochemical studies of arcs that have not incorporated B data; thus, measurements and modeling of B isotope systematics may reveal a variety of important insights into subduction zone processes.

Here we report $\delta^{11}B$ and Be/B ratios measured by secondary ion mass spectrometry (SIMS) in olivine-hosted melt inclusions (MIs) from Nicaraguan volcanoes and present a numerical dehydration model to investigate the origins of the measured compositions. Rear-arc samples from El Salvador (Tonarini et al., 2007) fall along the same broad mixing trend as our samples, indicating that the rear arc does not sample an isotopically distinct slab component. Our model demonstrates that fluids and melts originating from AOC and sediment alone can account for $\delta^{11}B$ in Nicaraguan volcanics, and that B from down-dragged forearc serpentinite or serpentinized lithospheric mantle is not required. In fact, to reproduce the B isotope ratios of the Nicaraguan slab component, the model can tolerate only small contributions from serpentinized mantle sources. Consequentially, if the subducting lithospheric mantle is heavily serpentinized (Ranero et al., 2003) most of the water stored in this layer may be transported to the deeper mantle.

2. Geological setting and samples

The samples in this study include Nicaraguan arc lavas and marine sediment from the Cocos plate, which is subducting beneath the arc with convergence rate of ~75 mm/yr and a ~60° dip angle (Syracuse and Abers, 2006). The subducting plate is ~25 Myr old and carries a ~200 m thick layer dominated by chalky carbonate overlain by ~200 m of hemipelagic diatomaceous mud (Aubouin et al., 1982; Plank and Langmuir, 1998). Despite limited variability in the bulk composition and thickness of offshore sediments (Plank, 2014) there are large regional variations in trace element ratios that appear to be controlled by variability in the recycling efficiency of the two sediment packages, which have very different compositions (Patino et al., 2000). The most pronounced variations occur in northwestern Nicaragua, where a negative correlation between Ba/Th and U/La in eruptive products is interpreted to reflect varying contributions from the two sediment endmembers to the arc (Fig. 2).

Six basaltic Nicaraguan lavas were selected for this study that span the full range of Ba/Th and U/La found in Nicaraguan lavas (Fig. 2). These samples have been previously analyzed for bulk rock major element, trace element, and radiogenic isotope data (Carr and Rose, 1987; Patino et al., 2000; Bolge et al., 2009). These data and other information about specific samples are available in the compilation of Carr et al. (2014). Four samples are from the region proximal to Telica volcano, including two from well preserved distal cones (TE116 and TE119) and two from the older Portillos lava flows (TE111 and TE113), which are slightly more evolved and lie northwest of the modern edifice. The other lavas samples include one from Masaya (MS7), and one from Cerro Negro (CN5), a polygenetic cinder cone whose eruptive products have notably high water contents (Gaetani et al., 2012; Roggensack et al., 1997). A whole-rock $\delta^{11}B$ measurement was also conducted on a new lava sample from the 1923 eruption of Cerro Negro, which is also the source of CN5. Four bulk samples of Cocos plate sediment were analyzed, with two each from the hemipelagic and carbonate layers cored by DSDP Hole 495, in order to assess whether differing subducting sediment compositions might influence $\delta^{11}B$ in the arc (Fig. 1).

Though some early studies (e.g., Walker et al., 1993) hypothesized that crustal assimilation could play a role in trace element and isotope variations within these volcanoes, numerous more recent geochemical studies of Nicaraguan volcanics have concluded that most regional variability in incompatible trace element and isotope ratios is representative of mantle wedge heterogeneity, which in most cases reflects variable contributions from the slab to the arc mantle source. Geochemical variability within individual volcanic centers is also mostly driven by either by local mantle wedge heterogeneity or crystal fractionation absent substantial crustal assimilation (e.g., Walker et al., 1993; Zurek et al., 2019; Pérez et al., 2020). The finding that regional geochemical variability is dominated by mantle rather than crustal processes is bolstered by the strong compositional relationship between the subducting sediment and geochemical systematics of the arc and the fact that the same regional systematics persist from basaltic to rhyolitic compositions (Patino et al., 2000; Vogel et al., 2006). Further discussion of this issue can be found in Neilsen et al. (2020), who measured thallium isotopes in an overlapping suite of samples. Though there is a general lack of evidence for crustal contamination of Nicaraguan basalts, additional precautions were taken to include the least differentiated samples possible in this study. Briefly, the selected samples lack significant Eu anomalies and have high CaO contents, precluding substantial plagioclase or clinopyroxene fractionation. While these samples are not 'primitive', this screening process should ensure that the selected samples were derived by <25% olivine-dominated crystal fractionation from a primary melt.

3. Methods

3.1. Melt inclusion preparation and analyses

MI-bearing olivines were hand-picked from the 0.5-1 mm size fraction of coarsely crushed and sieved lava samples. Olivines were then heated at either 1150 °C or 1200 °C (Table S1) in a 1-atm

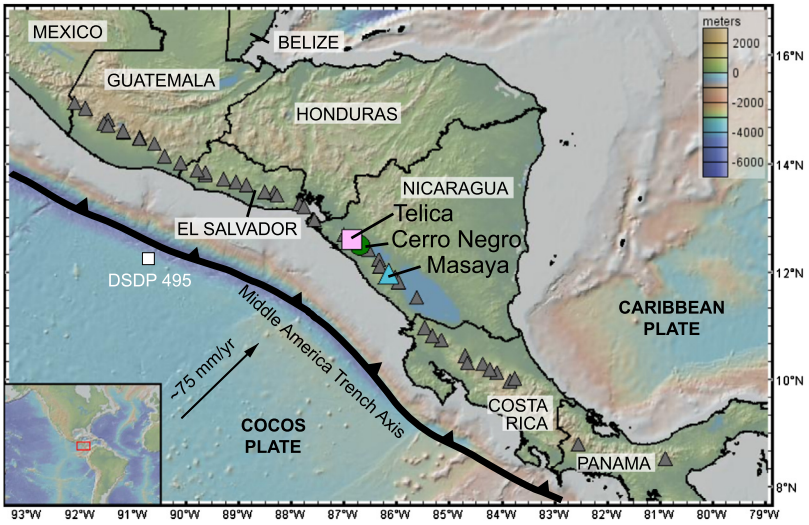

Fig. 1. Geologic setting. Gray triangles represent the volcanic front in Central America. The pink square, green circle, and blue triangle mark the respective locations of Telica, Cerro Negro, and Masaya. Also shown are the location of DSDP Hole 495, the Middle America trench axis, the angle of subduction, and the rate of subduction. Base map image is the Global Multi-Resolution Topography (GMRT) synthesis. Figure constructed using GeoMapApp version 3.6.10 in a Mercator projection.

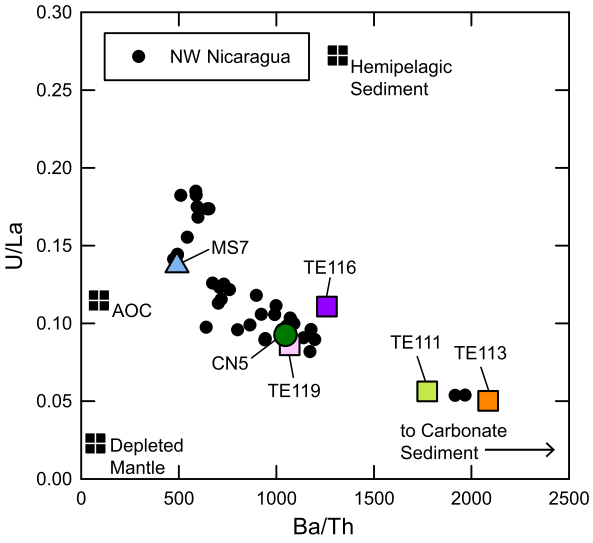

Fig. 2. Regional variations in Ba/Th and U/La in Nicaraguan lavas and Cocos plate samples. Data are from Cosiguina, San Cristobal, Telica, Rota, Cerro Negro, Las Pilas, Momotombo, Nejapa, and Masaya volcanoes alongside bulk sediment values from the Cocos plate (Bolge et al., 2009; Patino et al., 2000; Heydolph et al., 2012) demonstrate regional geochemical trends in NW Nicaragua. Patino et al. (2000) show that these geochemical variations are best explained by variable inputs from carbonate vs. hemipelagic sediment. Anomalous "high Nb" (>3 ppm Nb) lavas and evolved samples (<4 wt.% MgO) are excluded, following Bolge et al., 2009, excepting samples from Telica's "Portillos" lava flow with 3-4 wt.% MgO due to their potential importance as the regional high-Ba/Th endmember. Depleted mantle values are N-MORB (Gale et al., 2013), altered oceanic crust (AOC). Carbonate sediment has Ba/Th = 13409 and U/La = 0.017.

gas mixing furnace using H_2/CO_2 gases to fix oxygen fugacity at one log unit above the quartz-fayalite-magnetite buffer. The goal of the reheating step was to maximize the size of glass inclusions available for analysis (rather than to restore the inclusions to their original composition) under the assumption that no B could be transferred into or out of the fully encapsulated inclusions. Single grains of olivine were then mounted in acrylic and ground to expose MIs, re-mounted in indium, and polished.

MIs and their host olivines were analyzed for major elements, sulfur (S), and chlorine (Cl) using the JEOL-JXA-8200 electron microprobe at Washington University. The MIs were subsequently analyzed for B and beryllium (Be) concentrations and B isotope ratios using the Cameca IMS 7f-geo ion probe at Washington University. Sample analyses were bracketed with analyses of a suite of silicate glass reference standards following Jones et al. (2014) and Walowski et al. (2019). A more detailed description of SIMS analyses is given in the Supplementary Information.

3.2. Whole-rock measurements

B concentrations were measured in two carbonate samples (24R and 37R) and two hemipelagic sediment samples (5R and 12R) from DSDP Hole 495 using a Thermo iCAP-Q quadrupole-inductively coupled plasma-mass spectrometer at Washington University. 100 mg of milled sediments and geostandards BCR-2, AGV-2, BHVO-2, DNC-1a, JB-2, G-2, and W-2a were dissolved in 2 mL of double-distilled HNO_3 and 500 µL of HF (200 µL for the carbonate samples) in Teflon beakers at 115 °C for 48 hours. Samples were evaporated to dryness at 70 °C, redissolved in 8 mL HNO_3, then diluted 5000x in 2% HNO_3 spiked with 3 ppb Ge, 3 ppb Tm, and 8 ppb Re as an internal standard. Excellent standard calibration curves indicate that the low-temperature evaporation successfully prevented B volatilization (Fig. S4).

The sediment samples and whole-rock lava sample were prepared and analyzed for $\delta^{11}B$ at the Istituto di Geoscienze e Georisorse of the Italian National Research Council (IGG-CNR) in Pisa (Italy), following the procedure described by Agostini et al. (2021). Boron was extracted by melting in Pt-Ir crucibles after addition of a K_2CO_3 flux followed by aqueous leaching of the resulting fusion cake. Boron was then extracted from this solution with a three-step (2 x anion and 1 x cation column) chemical separation procedure, collected in 2% HNO_3, and measured on a Thermo Neptune Plus MC-ICP-MS with a procedure of sample-reference bracketing using NIST SRM 951 and an on-peak zero blank correction. Within-run errors on individual runs (n = 3) were in the order of 0.1±0.2‰. Several samples and in-house standards were re-processed and re-produced the original values within 0.4‰ or better (Agostini et al., 2021).

4. Results

A total of 39 MIs were prepared and analyzed following the methods described above and in the Supplementary Information (Sections S1, S2, and S3), though two analyzed inclusions (from TE113 and TE116) were apparently not fully encapsulated during

Table 1
Average B and Be abundances and δ^{11}B compositions in MIs from this study.

Volcano	Telica								Cerro Negro		Masaya	
Sample	TE111 (n = 2)		TE113 (n = 2)		TE116 (n = 5)		TE119 (n = 3)		CN5 (n = 11)		MS7 (n = 4)	
	avg.	std. dev.	avg.	std. dev.	avg.	std. dev.	avg.	std. dev.	avg.	std. dev.	avg.	std. dev.
B (ppm)	21.5	0.3	18.2	0.1	23.0	0.9	12.5	0.7	15.6	2.0	16.6	1.5
Be (ppm)	1.027	0.038	0.585	0.095	0.527	0.101	0.504	0.067	0.379	0.066	0.691	0.093
δ^{11}B (‰)	1.8	0.03	4.1	0.4	4.6	0.8	5.1	0.9	4.2	1.4	2.2	2.8

reheating and appear to have lost volatile elements (e.g., S and Cl) during the heating procedure (Section S4, and Fig. S8). These inclusions are characterized by rough, irregular boundaries with their host olivines and have obvious vesicles and cracks on their boundaries, as well as anomalously low B abundances (<10 ppm) and much higher δ^{11}B than other MIs from the same samples (>8.0‰). These analyses have thus been excluded from further interpretation. One other inclusion (as well as its host olivine) from Masaya was compositionally anomalous compared to the extensive melt inclusions data from other Masaya studies (Pérez et al., 2020; Zurek et al., 2019), and likely xenocrystic (Section S5, Fig. S7). Another subset of rehomogenized inclusions have SiO_2 contents as low as 42.30 wt.% SiO_2 (Section S4, Fig. S5), which is well outside the range of published whole rock and MI analyses for these volcanoes (Robidoux et al., 2017; Sadofsky et al., 2008; Zurek et al., 2019) and many have compositions that are nepheline normative. This is best explained by coupled H_2O and SiO_2 loss during heating, as documented by Portnyagin et al. (2019). Because coupled loss of B and H from olivine-hosted MIs has also been identified (Ingrin et al., 2014), it is possible that the δ^{11}B measurements in these rehomogenized inclusions are not representative of the magmas that were originally entrapped. And indeed, the lowest SiO_2 inclusions are offset to lighter δ^{11}B by about 1.9‰ relative to those with no evidence of Si-loss. While we have excluded these 14 low-SiO_2 inclusions from further interpretation, keeping them would have lowered the average projected subduction component composition (discussed below) by only ~0.5‰ δ^{11}B, however, and have a negligible impact on our data interpretation and modeling.

The average δ^{11}B for the remaining Nicaraguan MI is +3.8 ± 1.8‰ (1σ), and the range of individual MI δ^{11}B analyses is −1.6 ± 1.9‰ (MS7) to +6.1 ± 1.8‰ (TE119). The δ^{11}B means, weighted by B abundance, and standard deviations for individual samples are +4.1 ± 0.4‰ for TE113 (2 analyses), +4.6 ± 0.8‰ for TE116 (5 analyses), +5.1 ± 0.9‰ TE119 (3 analyses), +4.2 ± 1.4‰ for CN5 (6 analyses), and +2.2 ± 2.8‰ for MS7 (4 analyses; Table 1; Fig. S12). The Cerro Negro whole-rock sample has δ^{11}B of 1.55 ± .004‰, which overlaps within the uncertainty of the individual Cerro Negro melt inclusion values. The measured Nicaraguan MI compositions – alongside whole-rock δ^{11}B data from recently erupted mafic and intermediate El Salvadorian arc volcanics (Tonarini et al., 2007) – broadly fit a two-component mixing trend between DMM (Marschall et al., 2017) and a B-rich slab-derived component ranging from +2.9‰ to +5.9‰ on a plot of Be/B versus δ^{11}B (Fig. 3).

Analyses of the DSDP Hole 495 sediments range from 22 to 28 ppm B and δ^{11}B of +2.9‰ to +3.7‰ for the carbonate-dominated sediment, and 82 to 110 ppm B and δ^{11}B +0.7‰ to +2.1‰ for the hemipelagic sediment (Table 2). The carbonate-dominated layer of the DSDP 495 sediments has significantly lighter δ^{11}B than other modern marine carbonates, which are typically >+20‰ δ^{11}B (Hemming and Hanson, 1992; Vengosh et al., 1991), and are similar in δ^{11}B to the shallower hemipelagic sediment layer. This suggests that biogenic materials do not contribute significantly to the B budget of either sediment package. The hemipelagic sediment δ^{11}B values measured here are consistent with other siliceous marine sediments (Ishikawa and Nakamura, 1993; Tonarini et al., 2011).

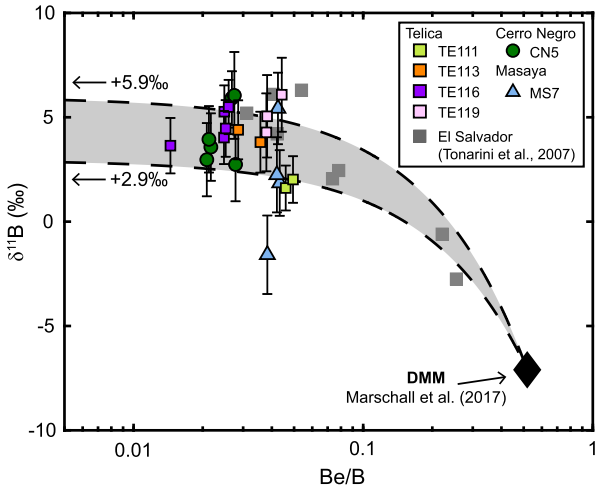

Fig. 3. Measured δ^{11}B and Be/B in MIs. Be/B and δ^{11}B from this study (Table 1). X axis is logarithmically scaled. Depleted MORB mantle (DMM) from Marschall et al. (2017). Linear mixing lines project from DMM to the average MI δ^{11}B ± 1σ (+2.9‰ to +5.9‰) and encompass the majority of the data. Gray squares indicate data on Salvadoran lavas from Tonarini et al. (2007). Note that one dacite and six older basement samples measured by Tonarini et al. (2007) are not included on this plot. MI and whole rock data from Nicaragua and El Salvador are broadly reproduced by linear mixing between a B-enriched, isotopically heavy slab-derived component and DMM. The B isotopic composition of MIs is dominated by the slab-derived component.

Table 2
B abundances and δ^{11}B of sediments from DSDP Hole 495.

Sample	495-5R	495-12R	495-24R	495-37R
Sediment Type	Hemi.	Hemi.	Carb.	Carb.
B (ppm)	82	110	28	22
δ^{11}B (‰)	2.1	0.7	2.9	3.7

5. Discussion

The range of B isotopic compositions measured in young mafic and intermediate lavas from Nicaragua and El Salvador are broadly consistent with mixing between a depleted mantle composition and a slab-derived component with δ^{11}B ranging from +2.9‰ to +5.9‰ (Fig. 3). De Hoog and Savov (2018) and Zhang et al. (2021) note a positive global correlation between arc δ^{11}B values and slab dip angle. The Nicaraguan slab dip angle is one of the steepest in the world (Syracuse et al., 2010), while Nicaraguan MI δ^{11}B compositions are generally lower than arc-front volcanics from other arcs (De Hoog and Savov, 2018). The Nicaraguan volcanics are therefore offset from the suggested global relationship between slab dip angle and δ^{11}B. While the δ^{11}B composition of the El Salvador-Nicaragua slab component generally overlaps with the compositions of Cocos plate sediments, it is unlikely that B from recycled sediment is the dominant control on the slab component, because the sediments dehydrate and release ^{11}B-enriched

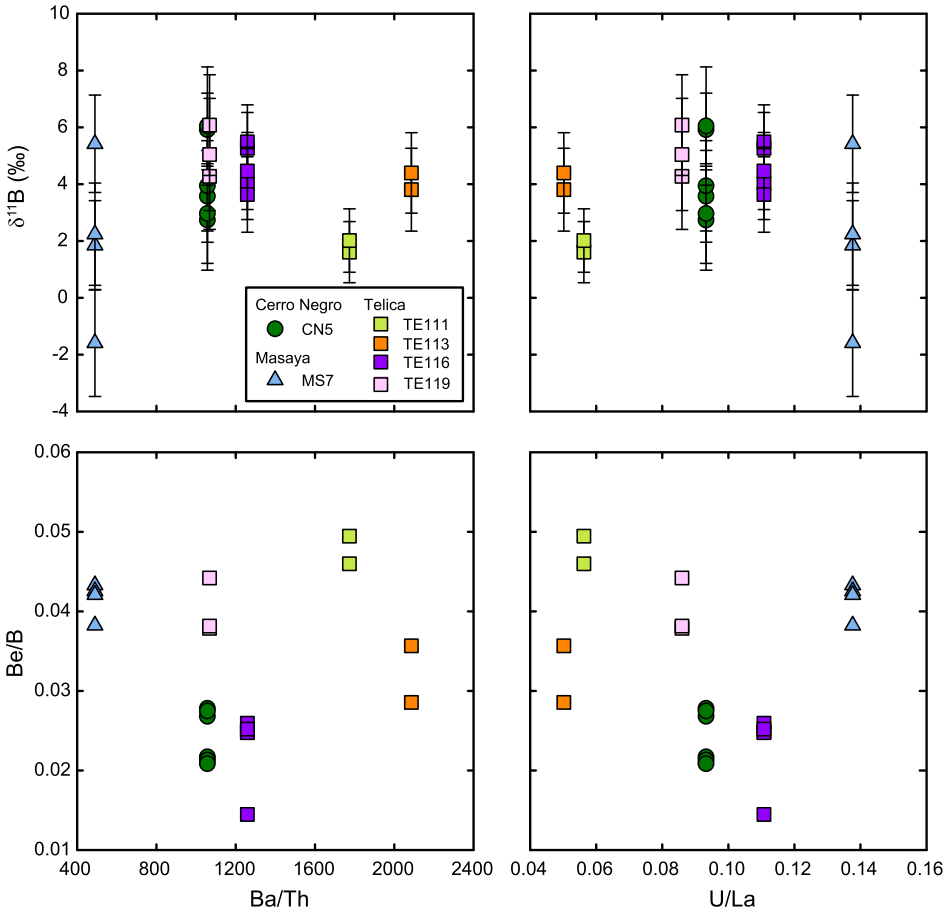

Fig. 4. The relationship of MI δ^{11}B to whole rock trace element ratios. δ^{11}B (panels **A** and mextbfB) and Be/B (panels **C** and **D**) of individual MIs (Table 1) plotted against whole rock Ba/Th and U/La from the same samples (Patino et al., 2000). There is a lack of correlation between δ^{11}B, Be/B and Ba/Th, U/La, suggesting that the relative proportion of carbonate sediment to hemipelagic sediment recycled from the slab to the arc controls neither the [B] nor the δ^{11}B of arc volcanics. This is consistent with the similar δ^{11}B compositions of the different sediments from DSDP Hole 495 (Table 2).

fluids beneath the forearc, resulting in lower δ^{11}B composition in the metasediment transported beneath the arc (van Keken et al., 2011; Savov et al., 2007). This inference is reinforced by the fact the trace element ratios U/La and Ba/Th, which are strongly controlled by the recycling efficiency of the sediment layers (Fig. 2, Patino et al., 2000), have no apparent relationship with measured δ^{11}B values (Fig. 4), despite large differences in the B abundances between the different sediment packages.

Some studies have suggested that high δ^{11}B values in arcs might instead result from "down-dragging" and subsequent dehydration of serpentinized forearc peridotite (Tonarini et al., 2007, 2011). It is unclear whether such a model is consistent with the low heat flux measured in fore-arc regions, however, which require limited mass transfer into and out of the fore-arc region (Wada and Wang, 2009). Alternatively, B measured in arcs could be sourced from deeper layers of the slab, including the subducting lithospheric mantle (Konrad-Schmolke et al., 2016; Cooper et al., 2020). It remains uncertain whether a significant amount of B can be transported through the oceanic crust to the slab mantle, however, without being incorporated by alteration reactions in the shallower ocean crust (McCaig et al., 2018).

Interpretations of B isotope data in arcs vary greatly, in part due to the multitude of factors influencing fractionation of B isotopes during slab dehydration, and in part because the initial B isotopic compositions of deep slab dikes, gabbros/troctolites, and altered peridotites are not well constrained. Studies such as Marschall et al. (2007), Jones et al. (2014), and Konrad-Schmolke et al. (2016) demonstrate that the complexity of the B isotope system can be addressed using numerical methods, but no study has yet evaluated the impact of uncertainties in the slab composition in tandem with a numerical approach. Below, we attempt to address this gap using a numerical model to evaluate whether the typical slab dehydration and melting processes thought to occur in most of the world's arcs might satisfactorily account for the observed range of δ^{11}B signatures in Central American volcanics.

5.1. Model description

The model developed here uses slab thermal models of van Keken et al. (2018) to estimate the sequence of slab dehydration, and resultant B fractionation and transport. An illustration of the model setup is shown in Fig. 5. The model uses a convergent rate and subduction geometry specific to Nicaragua. The thermal models introduce variable amounts of slab surface heating consistent with the effects of shear heating. We utilize models with either no shear heating (the $f_{arbi} = 0$ model of van Keken et al., 2018) or moderate shear heating ($f_{arbi} = 2$ model) that are generally consistent with fore arc heat flow measurements (van Keken et al., 2018).

The dehydration model generally follows the approach of van Keken et al. (2011, 2018). The maximum structurally bound water that can remain in pelite, MORB, and mantle lherzolite at a given P and T is determined using the petrological models of Hacker (2008), which are provided as P-T-H_2O grids by Kimura (2017). Initial H_2O contents in the layers of the basaltic crust are based on the model of Jarrard (2003), while the sediment is treated as a sin-

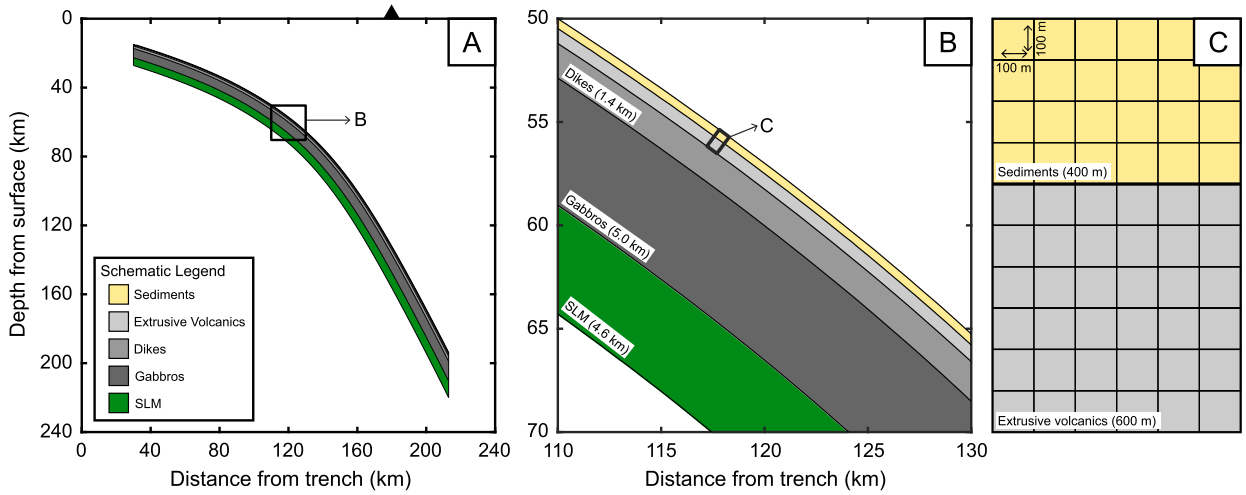

Fig. 5. Illustration of dehydration model setup. Subducting lithologies are color-coded as follows: sediments are beige, extrusive volcanics are light gray, sheeted dikes are medium gray, gabbros are dark gray, and serpentinized lithospheric mantle (SLM) is forest green. **A:** The complete area spanned by the model. A black box denotes the region shown in panel B. The location of the arc front (178.3 km from the trench; Syracuse and Abers, 2006) is noted with a black triangle. **B:** A zoomed-in view of the modeled slab, highlighting the different lithologies and their thicknesses. A black box denotes the region in panel C. **C:** A zoomed-in view of the sediment and extrusive volcanic lithologies in the model slab, and individual grid cells, which measure 100 m × 100 m. Sediments are shown as ∼400 m thick, but in the model they are 200 m thick to correct for density differences between sediments, altered oceanic crust (AOC), and SLM.

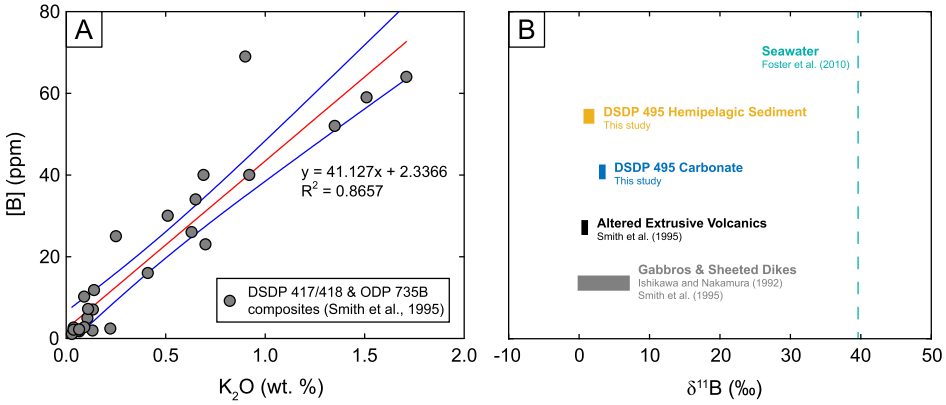

Fig. 6. The initial B abundances and B isotopic compositions of subducting materials in our dehydration model. A: K_2O and B content of composites sampled at DSDP Holes 417, 418 (extrusive volcanics) and ODP site 735B (gabbros). Red line is a linear least-squares fit to the data and blue curves are 95% confidence intervals. We use this positive correlations and the K_2O model of Jarrard (2003) to estimate initial B content in subducting AOC. **B:** Ranges of $\delta^{11}B$ measured in subducting lithologies. Sediment ranges were determined in this study. Two samples of DSDP 495 hemipelagic sediment were determined to have $\delta^{11}B = +2.1‰$ and $+0.7‰$. Two samples of DSDP 495 carbonate were determined to have $\delta^{11}B = +2.9‰$ and $+3.7‰$. Initial bulk sediment $\delta^{11}B$ is then determined by taking the weighted average $\delta^{11}B$ of these four samples. Extrusive volcanics have $\delta^{11}B = +0.4‰$ to $+1.2‰$ (Smith et al., 1995). The compositional range measured in gabbros and sheeted dikes (Ishikawa and Nakamura, 1992; Smith et al., 1995) range from $\delta^{11}B = -0.1‰$ to $+7.1‰$. For reference, the $\delta^{11}B$ of seawater is also shown ($+39.61‰$; Foster et al., 2010).

gle unit with 3.24% H_2O (Patino et al., 2000). As the slab subducts, the maximum amount of structurally bound water that can be held in each layer decreases, with excess water converted to fluid. If the total fluid fraction exceeds 0.1 wt.% in a given grid cell, the fluid is removed from the slab.

Partitioning of B between fluids and residual solids depends on the mineral phengite, which is the dominant solid reservoir for B (Marschall et al., 2007). The proportion of phengite in each grid cell is determined by the K_2O content, which for the mafic crust we again set using the alteration model of Jarrard (2003), and for the sediment a bulk composition based on Patino et al. (2000). We assume phengite is exhausted from the sediment layers at 850 °C as a result of sediment melting, consistent with the experiments of Skora and Blundy (2010).

The initial B concentration in the mafic crust was estimated based on the correlation between B and K_2O content (Fig. 6a) in the data of Smith et al. (1995), a notable improvement from previous modeling efforts that assumed a uniform 25 ppm B throughout the mafic crust (Konrad-Schmolke et al., 2016). Measurements of $\delta^{11}B$ in the different layers of the ocean crust (Ishikawa and Nakamura, 1992; Smith et al., 1995), however, have produced varied results. To address this uncertainty, models were run using initial $\delta^{11}B$ distributions that encompassed the full range of measured compositions from each layer of the ocean crust (Fig. 2b).

Whenever a fluid is present in the slab, the B concentrations of the fluid and residual solids are calculated using a bulk partition coefficient based on the amount of phengite present. $\delta^{11}B$ compositions in fluids and residual solids are then calculated using the temperature dependent fractionation equation of Wunder et al. (2005) and basic mass balance. Additional model details and specific equations are available in supplement S7.

5.1.1. Model results: residual slab compositions

As the slab subducts, water is lost from progressively deeper slab layers. The progressive extraction of fluids or melts from the slab leaves the slab residuum depleted in ^{11}B (De Hoog and Savov, 2018; Peacock and Hervig, 1999; Rosner et al., 2003). Model results for the slab H_2O, B, and $\delta^{11}B$ (Fig. 7) show how slab compositions evolve during subduction. These diagrams depict a flat projection

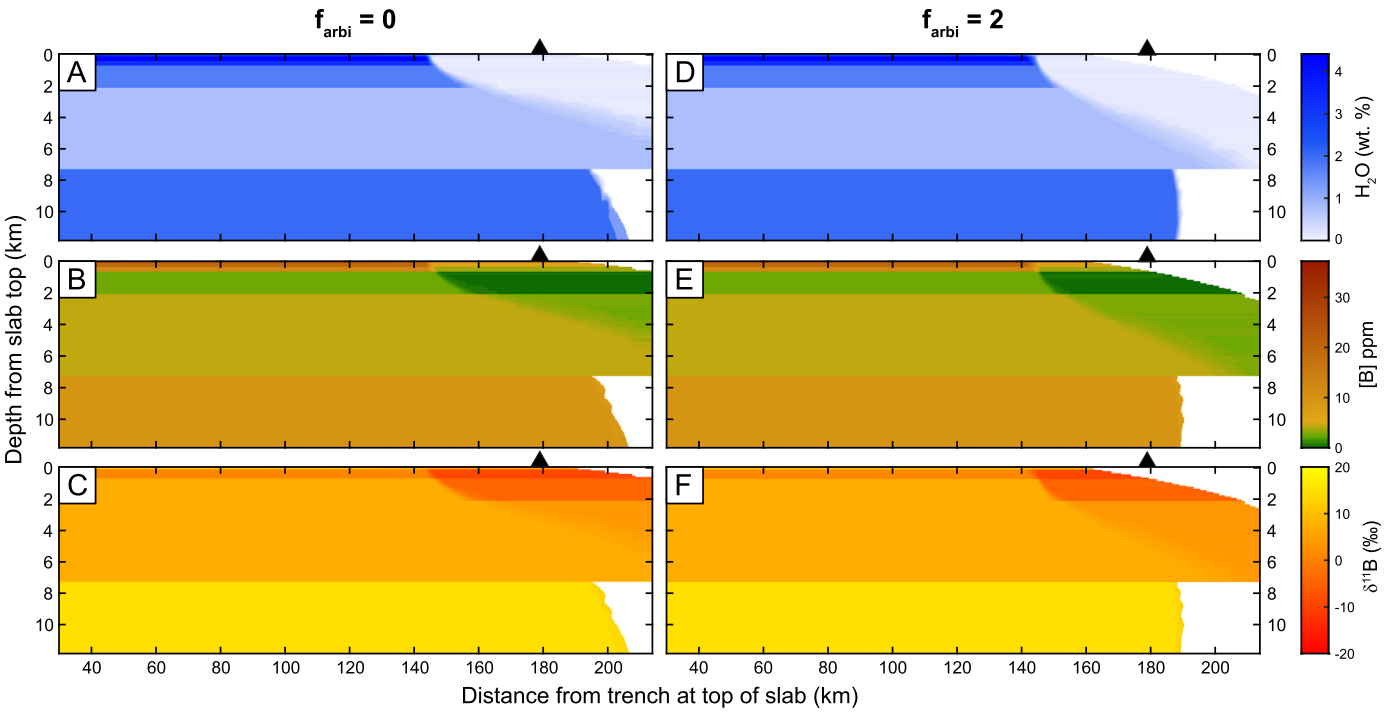

Fig. 7. Residual slab H_2O concentration, boron concentration and boron isotopic profiles. A comparison of subducting slab compositions for $f_{arbi} = 0$ (panels **A**, **B**, and **C**) and $f_{arbi} = 2$ (panels **D**, **E**, and **F**). **A & D:** H_2O content. **B & E:** [B] in ppm. **C & F:** $\delta^{11}B$ in ‰. In all panels, white areas represent regions of the slab that have undergone full H_2O and B loss. Depth from the slab top is on the y axis and extends from 0 to 11.8 km. The x-axis shows distance from the trench at the top of the slab. As in van Keken et al. (2018, 2011), the slab H_2O content, [B], and $\delta^{11}B$ are displayed by projecting the model coordinates into a slab reference frame where all layers have the same distance from the trench as the top of the slab. The location of the arc front (178.3 km from the trench; Syracuse and Abers, 2006) is noted with black triangles. B abundances and $\delta^{11}B$ for single layers in the model using $f_{arbi} = 0$ and $f_{arbi} = 2$ are similar, which suggests that the extent of B isotopic fractionation in residual slab layers remains the same under different levels of shear heating. Additionally, significant quantities of B and H_2O are retained in the slab past depths of arc magma generation.

of the slab based on the distance of vertical columns of the slab from the trench (see Fig. 5), as also utilized by van Keken et al. (2011, 2018). The Nicaraguan $f_{arbi} = 0$ and $f_{arbi} = 2$ models, which correspond to either no shear heating or moderate shear heating, produce similar overall results (Fig. 7). This occurs because the temperature variations imposed by a reasonable amount of shear heating are largely confined to the uppermost layers of the slab (van Keken et al., 2018). The primary difference between the two shear heating models is that the temperature threshold for phengite-out via sediment melting occurs slightly earlier in the hotter $f_{arbi} = 2$ model (Fig. 7d).

In both shear heating scenarios, layers that fully dehydrate reach a similar final $\delta^{11}B$. The sediment layers have an initial $\delta^{11}B$ of +1.7‰, with final $\delta^{11}B$ values of −3.6‰ to −3.3‰. Considering the full range of starting values, the final $\delta^{11}B$ of extrusive volcanics ranges from −8.9‰ to −9.7‰ for $f_{arbi} = 0$ and −9.1‰ to −9.9‰ for $f_{arbi} = 2$. The lower layers of the oceanic crust remain hydrated in $f_{arbi} = 0$, but the dikes and the uppermost 0.8 km of the gabbro layer dehydrate completely in $f_{arbi} = 2$. In this latter scenario, dehydrated dikes have $\delta^{11}B$ ranging from −11.7‰ to −4.5‰ and gabbros have a final $\delta^{11}B$ ranging from −3.5‰ to +3.7‰. The bulk slab $\delta^{11}B$ following dehydration, including layers that do not fully dehydrate, is −4.3‰ to +2.1‰ for $f_{arbi} = 0$ and −5.5‰ to +0.5‰ for $f_{arbi} = 2$. We note that the lowest $\delta^{11}B$ of dehydrated dikes in the residual slab is similar to the heaviest $\delta^{11}B$ of deeply recycled components suggested to manifest in the B isotopic compositions of hotspots studied by Walowski et al. (2019). Further dehydration or loss of B beyond the arc will result in $\delta^{11}B$ for residual oceanic crust that is well within the range of $\delta^{11}B$ for deeply recycled materials (Konrad-Schmolke and Halama, 2014; Walowski et al., 2019). This model result may indicate that dehydrated lower oceanic crust carries B to the deep mantle (see Section 5.2).

5.1.2. Model results: aggregated fluid compositions

There is substantial uncertainty regarding the pathways that slab-derived fluids may take through the mantle wedge, though the slab components transferred to the arc likely originate from the slab across a range of depths rather than from the slab directly beneath the arc. It is possible, for example, that materials lost from the slab at shallow depths continue to move downwards in areas of low porosity, or that slab liquids generated at great depths can migrate back toward the arc front (e.g., Cerpa et al., 2017; Wilson et al., 2014). In general, the thermal models used here are designed to be consistent with fore-arc heat flow data, which requires a rapid transition from decoupled to coupled behavior between the slab and overlying mantle wedge at ∼80 km depth (Wada and Wang, 2009; Syracuse et al., 2010). Following this logic, we assume any fluids lost beneath the forearc are not mixed into the hot mantle wedge beneath the arc. In our model results, we thus track the composition of continuously aggregated fluids lost prior to the depth of slab-mantle coupling separately from those lost beyond this point.

The observation that two-component mixing between generally uniform slab and mantle components can account for the arc $\delta^{11}B$ data suggests that the slab component transported to the arc is reasonably well mixed, even though the incremental products of slab dehydration may vary. Fluids or melts extracted from the slab across a range of depths may be transported into the source region of arc magmas, though the bounds on this depth range are not well constrained. There is some depth beyond which any remaining water (and B) in the slab is retained and transported more deeply into the mantle rather than back toward the arc. Given that this cut-off depth is unknown, we opted to continuously track the aggregated compositions of fluids lost from the slab starting from the slab-mantle coupling depth. Each individual aliquot of liquid lost from the slab as it continues to dehydrate is added to a bulk fluid com-

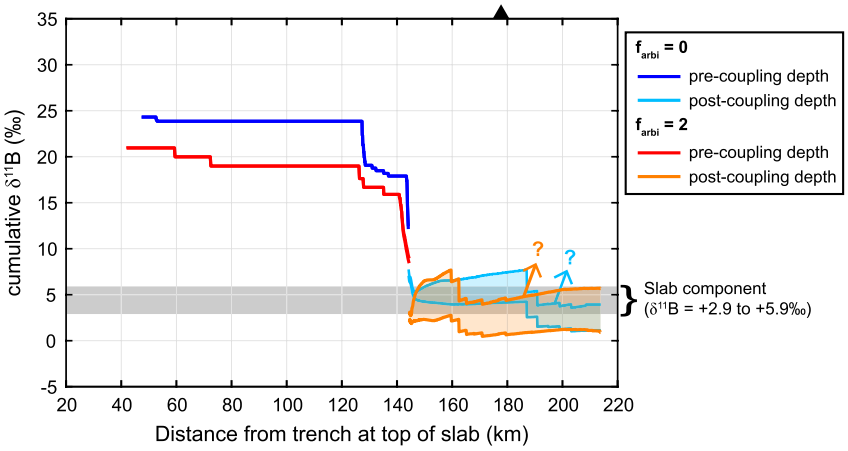

Fig. 8. Cumulative δ^{11}B in slab-derived fluids. The cumulative fluid δ^{11}B is tracked for all fluids released before the coupling depth, which likely contribute to the fore-arc (blue and red), and is tracked separately for fluids released beyond the coupling depth, which likely contribute to the arc (orange and cyan zones). Results are shown for shear heating scenarios $f_{arbi} = 0$ and $f_{arbi} = 2$. Bold curves are the highest and lowest possible fluid δ^{11}B, with the shaded regions showing the full range of potential cumulative fluid δ^{11}B. Slab-derived fluid compositions prior to the coupling depth are not shaded because they are dominated by sediment contributions; sediments are assigned a single initial δ^{11}B, and thus do not produce a range of slab-derived fluid δ^{11}B. Dark and light blue curves show the δ^{11}B of cumulative fluids before and after the coupling depth, respectively, for $f_{arbi} = 0$. Red and orange curves show cumulative fluid δ^{11}B before and after the coupling depth, respectively, for $f_{arbi} = 2$. Blue and orange arrows show the potential contributions of SLM-derived fluids; their locations indicate the beginning of the antigorite-out reaction. The range of δ^{11}B of the slab component (+2.9 to +5.9‰) is indicated by a gray bar on the plot. The location of the arc front (178 km from the trench; Syracuse and Abers, 2006) is noted with a black triangle. In both shear heating scenarios, our model results for aggregated fluids released past the coupling depth closely resemble the δ^{11}B of MIs from Telica, Cerro Negro, and Masaya. Beyond the coupling depth, slab-derived material originating from subducted AOC and, to a lesser extent, subducted sediments overlap the range of δ^{11}B measured in arc volcanics. Thus, the majority of slab-derived B is supplied to the arc by these lithologic units.

position. If the aggregated fluid composition intersects the average composition of the subduction component defined by the arc data (Fig. 3), then the model is considered consistent with available observations.

Fig. 8 shows the isotopic evolution of aggregated fluids released from the slab either prior to the depth of coupling (i.e., the contributions to the forearc) or beyond the depth of coupling (potential contributions to the arc). In the forearc, slab-derived fluids are primarily released from sediment layers, with minor contributions from the upper oceanic crust as the slab approaches the coupling depth. The aggregated fluids released in the forearc have δ^{11}B ranging from $\sim +15‰$ to $+25‰$ (Fig. 8), consistent with studies of forearc mud volcanoes in the Marianas (Benton et al., 2001). Beyond the coupling depth, fluids originating from the lower oceanic crust (i.e., dikes and gabbros) dominate the budget of slab-derived B. The modeled δ^{11}B composition of aggregated fluids released beyond the forearc quickly drops to overlap the range of δ^{11}B measured in Nicaraguan arc volcanics ($+2.3‰$ to $+5.7‰$) and stays in this range across the remainder of the model domain (Fig. 8). The ranges in model δ^{11}B values for each shear heating scenario (orange and cyan in Fig. 8) arise from the uncertainty associated with the initial δ^{11}B composition of the mafic ocean crust. The aggregated fluid lost beneath the forearc is slightly lighter for the shear-heating model, as expected from the hotter temperatures within the sediment layers. Beyond the forearc, the models largely overlap, but diverge slightly for aggregated fluids between 160 and 190 km from the trench because shear heating results in earlier phengite consumption via sediment melting.

The aggregated fluid compositions plotted on Fig. 8 do not incorporate the potential B flux from the lithospheric mantle of the subducting slab due to the inherent complexity of this process. Antigorite is predicted to dehydrate in the slab lithospheric mantle near the arc front, but it is possible that fluids produced by antigorite dehydration do not efficiently reach the mantle wedge. Chlorite can remain stable to much higher temperatures in bulk peridotite lithologies (Grove et al., 2012; Spandler et al., 2014), and the lower layers of the mafic crust have the potential to consume a large budget of H_2O via rehydration reactions as long as P-T conditions remain within the lawsonite stability field (Wada et al., 2012). As demonstrated by Wada et al. (2012), the ability for dehydration fluids from these lower slab layers to transect the over-riding peridotite and gabbro without being consumed by additional rehydration reactions depends on the extent of initial serpentinization and the specific distribution of hydrated layers within the subducting lithospheric mantle. Given these considerations, the potential effects of adding these antigorite breakdown fluids to the aggregate fluid composition of the rest of the slab are best considered independently.

5.2. Model implications

Our model successfully reproduces the compositional range of the subduction component defined by Nicaraguan and El Salvadorian arc volcanics with a slab flux that is dominated by fluids from the ocean crust and without the incorporation of any B from the subducting lithospheric mantle. This result can also be used to calculate an upper limit on the total amount of B that could conceivably be transported from subducting serpentinite. These constraints apply equally to serpentinite in the slab lithospheric mantle and serpentinite down-dragged from the forearc, as both have been ascribed a similar, and notably heavy, compositional range from $\delta^{11}B = +14‰$ to $\delta^{11}B = +20‰$ (Agranier et al., 2007; Benton et al., 2001; Tonarini et al., 2007, 2011; Marschall, 2018). For example, *assuming the absolute minimum* δ^{11}B values for all layers of the mafic ocean crust, and forearc serpentinite with $\delta^{11}B = +20‰$, a maximum of 18% of total slab-derived B could originate from these materials without exceeding the average δ^{11}B in the arc volcanics. This increases to a maximum of 25% serpentinite-derived B if the serpentinite has $\delta^{11}B = +14‰$. If the heaviest ocean crust δ^{11}B values are considered instead, however, there is essentially no capacity for a serpentinite-derived B flux to the arc, as is also apparent from the fact that the modeled maximum δ^{11}B fluid values added to the mantle wedge already hug the upper limit of the arc data (Fig. 8). By comparison, if the subducting lithospheric mantle carries ~10 ppm B in a layer that is 4.6 km thick, as in Fig. 5, this would account for about 50% of the subducting slab's total B budget. If significant heavy B is in fact subducted as serpentinite, our

model therefore indicates that some mechanism must prevent its large-scale transport to the arc mantle source.

The finding of limited B contributions from serpentinized mantle contrasts with the conclusions of several prior studies in El Salvador and elsewhere (Leeman et al., 2017; Savov et al., 2007; Tonarini et al., 2011, 2007). Our interpretation differs mostly due to an improvement in our understanding of slab thermal profiles and potential fluid pathways in the mantle wedge. For example, Tonarini et al. (2007) reasonably assumed that the upper layers of the slab (both sediment and AOC) would dehydrate entirely beneath the forearc, whereas more recent thermomechanical models do not support this suggestion (van Keken et al., 2018, 2011). Another important development stems from an improved understanding of the possible transport pathways available to fluids and melts after they are produced, and the fact that the arc mantle source is not necessarily sampling fluids produced in a narrow range directly beneath the arc (Cerpa et al., 2017; Wilson et al., 2014). Our interpretation also benefits from consideration of the uncertainty associated with the composition of the oceanic crust, as well as the use of the relationship between B and K_2O compositions in ocean floor drill cores.

There are several possible areas for future development of this modeling approach. For example, our model assumes perfect mixing of aggregated slab-derived fluids beyond the coupling depth, but fluids probably mix to variable degrees and leave a heterogeneous signature on arc mantle sources. This could partially explain the variation seen among individual melt inclusions and samples. This mixing assumption underpins the decision to compare the aggregated slab fluid to the inferred average value of the B-rich subduction component (Fig. 3) rather than to individual samples or MIs. There may also be heterogeneities in MI compositions due to local variations in the composition of slab materials. Indeed, one MI analysis from Masaya with the lowest $\delta^{11}B$ does not overlap with the range of model results. Some of the older El Salvadorian basement samples measured by Tonarini et al. (2007) also fall outside of the model range. Though these caveats highlight important additional considerations, they do not impact our overall interpretation of the arc volcano compositions as modeled, which should relate specifically to the average composition of the mantle wedge sampled by the arc.

While our model does not incorporate the potential effects of fluid-rock reaction during fluid ascent through the slab and mantle wedge, a preliminary exploration indicates that the net effect would be subtle for the Nicaraguan slab geometry. This is primarily because most B is already partitioned into fluids as they are produced during dehydration reactions, as can be seen on Fig. 7. Because there is little B left in the dehydrated portions of the slab, fluid interaction with this rock has only a minor impact on the fluid $\delta^{11}B$. Fluid-rock reaction would have a more prominent effect in layers with substantial phengite, and hence a larger rock/fluid bulk partition coefficient for B, though both $f_{arbi} = 0$ and $f_{arbi} = 2$ temperature profiles indicate that most phengite near the slab surface will be consumed during sediment melting shortly after the slab passes from the forearc to the mantle wedge. A more detailed treatment of fluid-rock reaction and slab melting are the subjects on ongoing work.

The model presented here also has implications for the transport of surface B and H_2O into the deep mantle. The $\delta^{11}B$ of dehydrated AOC layers in the residual slab are $-11.7‰$ to $+0.5‰$; the lightest isotopic composition retained in the dehydrated crust is similar to the heaviest $\delta^{11}B$ of deeply recycled components inferred from the B isotopic compositions of hotspot samples (Walowski et al., 2019). We note that the maximum amount of water retained in the sediments and AOC layers (in the scenario with no shear heating) would be 250 ppm if averaged over 100 km of slab, slightly below the concentration range estimated for the Phanerozoic global average slab residuum to the deep mantle from Parai and Mukhopadhyay (2012), assuming a near steady-state ocean (0-100 m sea level decrease). Outer rise bend faults may extend through the lower crust and into the slab mantle in the Cocos plate (Ranero et al., 2003) and may provide pathways for seawater interaction with the slab lithospheric mantle, though the extent of serpentinization may be limited by low porosity and low fluid flux through the lithospheric mantle (Naif et al., 2015). If the Cocos slab mantle is extensively serpentinized, it may carry significant additional B and H_2O. Our model results indicate that serpentinite-derived B is not efficiently transported to regions of magma generation at Nicaragua; if B tracks H_2O transport in the subduction zone, then serpentinized lithospheric mantle in the residual slab may carry a significant amount of H_2O into the deep mantle.

6. Conclusion

We measured B and Be concentrations and $\delta^{11}B$ in Nicaraguan MIs and developed a numerical model of slab dehydration to interpret our new dataset. The compositions of these MIs are consistent with a slab-derived component that has $\delta^{11}B$ ranging from $+2.9‰$ to $+5.9‰$. We also measured the $\delta^{11}B$ values of subducted carbonate and hemipelagic sediments from DSDP Hole 495 on the Cocos plate are $+3.3‰$ and $+1.3‰$ (<0.5% uncertainty), respectively. We developed a model to better understand the origin of Nicaraguan MI $\delta^{11}B$ compositions that accounts for the initial compositions of subducting lithologies on the Cocos plate, the thermochemical structure of the Nicaraguan subduction zone, and the expected fractionation of B isotopes as a function of temperature. The aggregated $\delta^{11}B$ of modeled slab-derived fluids from beyond the coupling depth closely matches the $\delta^{11}B$ of Nicaraguan MIs without contributions of fluids from the slab mantle and down-dragged forearc serpentinite. Instead, subducted AOC likely provides the majority of slab-derived fluids and B to the volcanic front of Nicaragua and El Salvador, with minor contributions from subducted sediments. This result remains robust when reasonable extents of shear heating are considered. Our findings suggest that serpentinite-derived fluids are not required to explain $\delta^{11}B$ of these olivine-hosted MIs, and place limits on their contribution to the B budget of arc magmas. Based on our data and model outputs, we argue that water, B, and other volatiles contributing to arc magmatism in Nicaragua and El Salvador originate from the uppermost portions of the subducting Cocos plate, whereas volatiles residing in the lower oceanic crust and slab mantle may be retained past depths of arc magma generation.

CRediT authorship contribution statement

Stephen J. Turner: Conceptualization, Formal analysis, Methodology, Project administration, Software, Supervision, Visualization, Writing – original draft, Writing – review & editing. **Mattison H. Barickman:** Formal analysis, Investigation, Writing – original draft. **Julian Rodriguez:** Investigation, Writing – original draft. **David A. Fike:** Writing – original draft. **Clive M. Jones:** Investigation, Methodology, Writing – original draft. **Kun Wang:** Investigation, Methodology, Writing – original draft. **Ivan P. Savov:** Funding acquisition, Investigation, Methodology, Resources, Writing – original draft, Writing – review & editing. **Samuele Agostini:** Investigation, Methodology, Resources, Writing – original draft. **Michael J. Krawczynski:** Investigation, Methodology, Resources, Supervision, Writing – review & editing. **Rita Parai:** Conceptualization, Formal analysis, Funding acquisition, Investigation, Methodology, Project administration, Resources, Software, Supervision, Visualization, Writing – original draft, Writing – review & editing.

Declaration of competing interest

The authors have no competing interests to declare.

Data availability

Data have been submitted as a supplement.

Acknowledgements

ST thanks Washington University in St. Louis for support via the Steve Fossett Postdoctoral Fellowship, IS thanks the ERASMUS+ Program for supporting his B isotope work at CNR-Pisa, SA thanks IGG-CNR fund P-CT0029. Generous support to MHB, ST and RP from the McDonnell Center for the Space Sciences is gratefully acknowledged. M.J.K. acknowledges support from National Science Foundation EAR Grant no. 2047960

Appendix A. Supplementary material

Supplementary material related to this article can be found online at https://doi.org/10.1016/j.epsl.2023.118289.

References

Agostini, S., Di Giuseppe, P., Manetti, P., Doglioni, C., Conticelli, S., 2021. A heterogeneous subcontinental mantle under the African–Arabian Plate boundary revealed by boron and radiogenic isotopes. Sci. Rep. 11, 11230. https://doi.org/10.1038/s41598-021-90275-7.

Agranier, A., Lee, C.-T.A., Li, Z.-X.A., Leeman, W.P., 2007. Fluid-mobile element budgets in serpentinized oceanic lithospheric mantle: insights from B, As, Li, Pb, PGEs and Os isotopes in the Feather River Ophiolite, California. Chem. Geol. 245, 230–241. https://doi.org/10.1016/j.chemgeo.2007.08.008.

Ancellin, M.-A., Samaniego, P., Vlastélic, I., Nauret, F., Gannoun, A., Hidalgo, S., 2017. Across-arc versus along-arc Sr-Nd-Pb isotope variations in the Ecuadorian volcanic arc. Geochem. Geophys. Geosyst. 18, 1163–1188. https://doi.org/10.1002/2016GC006679.

Aubouin, J., von Huene, R., et al., 1982. Initial Reports of the Deep Sea Drilling Project, 67, Initial Reports of the Deep Sea Drilling Project. U.S. Government Printing Office.

Benton, L.D., Ryan, J.G., Tera, F., 2001. Boron isotope systematics of slab fluids as inferred from a serpentine seamount, Mariana forearc. Earth Planet Sci Lett 187, 273–282. https://doi.org/10.1016/S0012-821X(01)00286-2.

Bolge, L.L., Carr, M.J., Milidakis, K.I., Lindsay, F.N., Feigenson, M.D., 2009. Correlating geochemistry, tectonics, and volcanic volume along the Central American volcanic front. Geochem. Geophys. Geosyst. 10. https://doi.org/10.1029/2009GC002704.

Bonatti, E., Lawrence, J.R., Morandi, N., 1984. Serpentinization of oceanic peridotites: temperature dependence of mineralogy and boron content. Earth Planet. Sci. Lett. 70, 88–94. https://doi.org/10.1016/0012-821X(84)90211-5.

Carr, M.J., Rose, W.I., 1987. CENTAM – A data base of Central American volcanic rocks. J. Volcanol. Geotherm. Res. 33, 239–240. https://doi.org/10.1016/0377-0273(87)90066-7.

Carr, M.J., Feigenson, M.D., Bolge, L.L., Walker, J.A., Gazel, E., 2014. RU_CAGeochem, a database and sample repository for Central American volcanic rocks at Rutgers University. Geosci. Data J. 1, 43–48. https://doi.org/10.1002/gdj3.10.

Cerpa, N.G., Wada, I., Wilson, C.R., 2017. Fluid migration in the mantle wedge: influence of mineral grain size and mantle compaction. J. Geophys. Res., Solid Earth 122, 6247–6268. https://doi.org/10.1002/2017JB014046.

Churikova, T., Wörner, G., Mironov, N., Kronz, A., 2007. Volatile (S, Cl and F) and fluid mobile trace element compositions in melt inclusions: implications for variable fluid sources across the Kamchatka arc. Contrib. Mineral. Petrol. 154, 217–239. https://doi.org/10.1007/s00410-007-0190-z.

Cooper, G.F., Macpherson, C.G., Blundy, J.D., Maunder, B., Allen, R.W., Goes, S., Collier, J.S., Bie, L., Harmon, N., Hicks, S.P., Iveson, A.A., Prytulak, J., Rietbrock, A., Rychert, C.A., Davidson, J.P., the VoiLA team, 2020. Variable water input controls evolution of the Lesser Antilles volcanic arc. Nature 582, 525–529. https://doi.org/10.1038/s41586-020-2407-5.

De Hoog, J.C.M., Savov, I.P., 2018. Boron isotopes as a tracer of subduction zone processes. In: Marschall, H., Foster, G. (Eds.), Boron Isotopes: The Fifth Element. Springer International Publishing, Cham, pp. 217–247.

Foster, G.L., Pogge von Strandmann, P.A.E., Rae, J.W.B., 2010. Boron and magnesium isotopic composition of seawater. Geochem. Geophys. Geosyst. 11, Q08015. https://doi.org/10.1029/2010GC003201.

Gaetani, G.A., O'Leary, J.A., Shimizu, N., Bucholz, C.E., Newville, M., 2012. Rapid reequilibration of H2O and oxygen fugacity in olivine-hosted melt inclusions. Geology 40, 915–918. https://doi.org/10.1130/G32992.1.

Gale, A., Dalton, C.A., Langmuir, C.H., Su, Y., Schilling, J., 2013. The mean composition of ocean ridge basalts. Geochem. Geophys. Geosyst. 14, 489–518.

Grove, T.L., Till, C.B., Krawczynski, M.J., 2012. The role of H2O in subduction zone magmatism. Annu. Rev. Earth Planet. Sci. 40, 413–439. https://doi.org/10.1146/annurev-earth-042711-105310.

Hacker, B.R., 2008. H $_2$ O subduction beyond arcs. Geochem. Geophys. Geosyst. 9, Q03001. https://doi.org/10.1029/2007GC001707.

Hemming, N.G., Hanson, G.N., 1992. Boron isotopic composition and concentration in modern marine carbonates. Geochim. Cosmochim. Acta 56, 537–543. https://doi.org/10.1016/0016-7037(92)90151-8.

Heydolph, K., Hoernle, K., Hauff, F., van den Bogaard, P., Portnyagin, M., Bindeman, I., Garbe-Schönberg, D., 2012. Along and across arc geochemical variations in NW Central America: evidence for involvement of lithospheric pyroxenite. Geochim. Cosmochim. Acta 84, 459–491. https://doi.org/10.1016/j.gca.2012.01.035.

Ingrin, J., Kovacs, I., Deloule, E., Balan, E., Blanchard, M., Kohn, S.C., Hermann, J., 2014. Identification of hydrogen defects linked to boron substitution in synthetic forsterite and natural olivine. Am. Mineral. 99, 2138–2141. https://doi.org/10.2138/am-2014-5049.

Ishikawa, T., Nakamura, E., 1992. Boron isotope geochemistry of the oceanic crust from DSDP/ODP Hole 504B. Geochim. Cosmochim. Acta 56, 1633–1639. https://doi.org/10.1016/0016-7037(92)90230-G.

Ishikawa, T., Nakamura, E., 1993. Boron isotope systematics of marine sediments. Earth Planet. Sci. Lett. 117, 567–580. https://doi.org/10.1016/0012-821X(93)90103-G.

Ishikawa, T., Tera, F., 1997. Source, composition and distribution of the fluid in the Kurile mantle wedge: Constraints from across-arc variations of BrNb and B isotopes 16.

Iveson, A.A., Humphreys, M.C.S., Savov, I.P., de Hoog, J.C.M., Turner, S.J., Churikova, T.G., Macpherson, Colin G., Mather, T.A., Gordeychik, B.N., Tomanikova, L., Agostini, S., Hammond, K., Pyle, D.M., Cooper, G.F., 2021. Deciphering variable mantle sources and hydrous inputs to arc magmas in Kamchatka. Earth Planet. Sci. Lett. 562, 116848. https://doi.org/10.1016/j.epsl.2021.116848.

Jarrard, R.D., 2003. Subduction fluxes of water, carbon dioxide, chlorine, and potassium. Geochem. Geophys. Geosyst. 4, 8905. https://doi.org/10.1029/2002GC000392.

Jones, R.E., De Hoog, J.C.M., Kirstein, L.A., Kasemann, S.A., Hinton, R., Elliott, T., Litvak, V.D., 2014. Temporal variations in the influence of the subducting slab on Central Andean arc magmas: evidence from boron isotope systematics. Earth Planet. Sci. Lett. 408, 390–401. https://doi.org/10.1016/j.epsl.2014.10.004.

Kessel, R., Schmidt, M.W., Ulmer, P., Pettke, T., 2005. Trace element signature of subduction-zone fluids, melts and supercritical liquids at 120–180 km depth. Nature 437, 724–727. https://doi.org/10.1038/nature03971.

Kimura, J.-I., 2017. Modeling chemical geodynamics of subduction zones using the Arc Basalt Simulator version 5. Geosphere GES01468.1. https://doi.org/10.1130/GES01468.1.

Konrad-Schmolke, M., Halama, R., 2014. Combined thermodynamic–geochemical modeling in metamorphic geology: boron as tracer of fluid–rock interaction. Lithos 208–209, 393–414. https://doi.org/10.1016/j.lithos.2014.09.021.

Konrad-Schmolke, M., Halama, R., Manea, V.C., 2016. Slab mantle dehydrates beneath Kamchatka-Yet recycles water into the deep mantle. Geochem. Geophys. Geosyst. 17, 2987–3007. https://doi.org/10.1002/2016GC006335.

Leeman, W.P., Sisson, V.B., 1996. Geochemistry of boron and its implications for crustal and mantle processes. Rev Mineral Geochem 33, 645–707.

Leeman, W.P., Tonarini, S., Chan, L.H., Borg, L.E., 2004. Boron and lithium isotopic variations in a hot subduction zone—the southern Washington Cascades. Chem. Geol. 212, 101–124. https://doi.org/10.1016/j.chemgeo.2004.08.010.

Leeman, W.P., Tonarini, S., Turner, S., 2017. Boron isotope variations in Tonga-Kermadec-New Zealand arc lavas: implications for the origin of subduction components and mantle influences. Geochem. Geophys. Geosyst. 18, 1126–1162. https://doi.org/10.1002/2016GC006523.

Marschall, H.R., 2018. Boron isotopes in the ocean floor realm and the mantle. In: Marschall, H., Foster, G. (Eds.), Boron Isotopes, Advances in Isotope Geochemistry. Springer International Publishing, Cham, pp. 189–215.

Marschall, H.R., Altherr, R., Rüpke, L., 2007. Squeezing out the slab — modelling the release of Li, Be and B during progressive high-pressure metamorphism. Chem. Geol. 239, 323–335. https://doi.org/10.1016/j.chemgeo.2006.08.008.

Marschall, H.R., Wanless, V.D., Shimizu, N., Pogge von Strandmann, P.A.E., Elliott, T., Monteleone, B.D., 2017. The boron and lithium isotopic composition of mid-ocean ridge basalts and the mantle. Geochim. Cosmochim. Acta 207, 102–138. https://doi.org/10.1016/j.gca.2017.03.028.

McCaig, A.M., Titarenko, S.S., Savov, I.P., Cliff, R.A., Banks, D., Boyce, A., Agostini, S., 2018. No significant boron in the hydrated mantle of most subducting slabs. Nat. Commun. 9, 4602. https://doi.org/10.1038/s41467-018-07064-6.

Naif, S., Key, K., Constable, S., Evans, R.L., 2015. Water-rich bending faults at the Middle America Trench. Geochem. Geophys. Geosyst. 16, 2582–2597. https://doi.org/10.1002/2015GC005927.

Nakamura, E., Campbell, I.H., Sun, S., 1985. The influence of subduction processes on the geochemistry of Japanese alkaline basalts. Nature 316, 55–58.

Nielsen, S.G., Shu, Y., Auro, M., Yogodzinski, G., Shinjo, R., Plank, T., Kay, S.M., Horner, T.J., 2020. Barium isotope systematics of subduction zones. Geochim. Cosmochim. Acta 275, 1–18. https://doi.org/10.1016/J.GCA.2020.02.006.

Parai, R., Mukhopadhyay, S., 2012. How large is the subducted water flux? New constraints on mantle regassing rates. Earth Planet. Sci. Lett. 317–318, 396–406. https://doi.org/10.1016/j.epsl.2011.11.024.

Patino, L.C., Carr, M.J., Feigenson, M.D., 2000. Local and regional variations in Central American arc lavas controlled by variations in subducted sediment input. Contrib. Mineral. Petrol. 138, 265–283. https://doi.org/10.1007/s004100050562.

Peacock, S.M., Hervig, R.L., 1999. Boron isotopic composition of subduction-zone metamorphic rocks. Chem. Geol. 160, 281–290. https://doi.org/10.1016/S0009-2541(99)00103-5.

Pérez, W., Freundt, A., Kutterolf, S., 2020. The basaltic plinian eruption of the ∼6 ka San Antonio Tephra and formation of the Masaya caldera, Nicaragua. J. Volcanol. Geotherm. Res. 401, 106975. https://doi.org/10.1016/J.JVOLGEORES.2020.106975.

Plank, T., 2014. The chemical composition of subducting sediments. In: Treatise on Geochemistry. Elsevier, pp. 607–629.

Plank, T., Langmuir, C.H., 1998. The chemical composition of subducting sediment and its consequences for the crust and mantle. Chem. Geol. 145, 325–394. https://doi.org/10.1016/S0009-2541(97)00150-2.

Portnyagin, M., Mironov, N., Botcharnikov, R., Gurenko, A., Almeev, R.R., Luft, C., Holtz, F., 2019. Dehydration of melt inclusions in olivine and implications for the origin of silica-undersaturated island-arc melts. Earth Planet. Sci. Lett. 517, 95–105. https://doi.org/10.1016/j.epsl.2019.04.021.

Ranero, C.R., Phipps Morgan, J., McIntosh, K., Reichert, C., 2003. Bending-related faulting and mantle serpentinization at the Middle America trench. Nature 425, 367–373. https://doi.org/10.1038/nature01961.

Robidoux, P., Rotolo, S.G., Aiuppa, A., Lanzo, G., Hauri, E.H., 2017. Geochemistry and volatile content of magmas feeding explosive eruptions at Telica volcano (Nicaragua). J. Volcanol. Geotherm. Res. 341, 131–148. https://doi.org/10.1016/j.jvolgeores.2017.05.007.

Roggensack, K., Hervig, R.L., McKnight, S.B., Williams, S.N., 1997. Explosive basaltic volcanism from Cerro Negro Volcano: influence of volatiles on eruptive style. Science 277, 1639–1642. https://doi.org/10.1126/science.277.5332.1639.

Rosner, M., Erzinger, J., Franz, G., Trumbull, R.B., 2003. Slab-derived boron isotope signatures in arc volcanic rocks from the Central Andes and evidence for boron isotope fractionation during progressive slab dehydration. Geochem. Geophys. Geosyst. 4, 9005. https://doi.org/10.1029/2002GC000438.

Ryan, J.G., Morris, J., Tera, F., Leeman, W.P., Tsvetkov, A., 1995. Cross-arc geochemical variations in the Kurile arc as a function of slab depth. Science 270, 625–627. https://doi.org/10.1126/science.270.5236.625.

Sadofsky, S.J., Portnyagin, M., Hoernle, K., van den Bogaard, P., 2008. Subduction cycling of volatiles and trace elements through the Central American volcanic arc: evidence from melt inclusions. Contrib. Mineral. Petrol. 155, 433–456. https://doi.org/10.1007/s00410-007-0251-3.

Savov, I.P., Ryan, J.G., D'Antonio, M., Fryer, P., 2007. Shallow slab fluid release across and along the Mariana arc-basin system: insights from geochemistry of serpentinized peridotites from the Mariana fore arc. J. Geophys. Res. 112, B09205. https://doi.org/10.1029/2006JB004749.

Scambelluri, M., Tonarini, S., 2012. Boron isotope evidence for shallow fluid transfer across subduction zones by serpentinized mantle. Geology 40, 907–910. https://doi.org/10.1130/G33233.1.

Scambelluri, M., Müntener, O., Ottolini, L., Pettke, T.T., Vannucci, R., 2004. The fate of B, Cl and Li in the subducted oceanic mantle and in the antigorite breakdown fluids. Earth Planet. Sci. Lett. 222, 217–234. https://doi.org/10.1016/j.epsl.2004.02.012.

Skora, S., Blundy, J., 2010. High-pressure hydrous phase relations of radiolarian clay and implications for the involvement of subducted sediment in arc magmatism. J. Petrol. 51, 2211–2243. https://doi.org/10.1093/petrology/egq054.

Smith, H.J., Spivack, A.J., Staudigel, H., Hart, S.R., 1995. The boron isotopic composition of altered oceanic crust. Chem. Geol. 126, 119–135. https://doi.org/10.1016/0009-2541(95)00113-6.

Spandler, C., Pettke, T., Hermann, J., 2014. Experimental study of trace element release during ultrahigh-pressure serpentinite dehydration. Earth Planet. Sci. Lett. 391, 296–306. https://doi.org/10.1016/J.EPSL.2014.02.010.

Spivack, A.J., Edmond, J.M., 1987. Boron isotope exchange between seawater and the oceanic crust. Geochim Cosmochim Acta 51, 1033–1043. https://doi.org/10.1016/0016-7037(87)90198-0.

Syracuse, E.M., Abers, G.A., 2006. Global compilation of variations in slab depth beneath arc volcanoes and implications. Geochem. Geophys. Geosyst. 7, Q05017. https://doi.org/10.1029/2005GC001045.

Syracuse, E.M., van Keken, P.E., Abers, G.A., 2010. The global range of subduction zone thermal models. Phys. Earth Planet. Inter. 183, 73–90. https://doi.org/10.1016/j.pepi.2010.02.004.

Tonarini, S., Agostini, S., Doglioni, C., Innocenti, F., Manetti, P., 2007. Evidence for serpentinite fluid in convergent margin systems: the example of El Salvador (Central America) arc lavas. Geochem. Geophys. Geosyst. 8, Q09014. https://doi.org/10.1029/2006GC001508.

Tonarini, S., Leeman, W.P., Leat, P.T., 2011. Subduction erosion of forearc mantle wedge implicated in the genesis of the South Sandwich Island (SSI) arc: evidence from boron isotope systematics. Earth Planet. Sci. Lett. 301, 275–284. https://doi.org/10.1016/j.epsl.2010.11.008.

Turner, S.J., Langmuir, C.H., 2022a. An Evaluation of Five Models of Arc Volcanism. Journal of Petrology 63. https://doi.org/10.1093/PETROLOGY/EGAC010.

Turner, S.J., Langmuir, C.H., 2022b. Sediment and ocean crust both melt at subduction zones. Earth Planet Sci Lett 584, 117424. https://doi.org/10.1016/J.EPSL.2022.117424.

Turner, S.J., Langmuir, C.H., 2022c. A quantitative framework for global variations in arc geochemistry. Earth Planet Sci Lett 584, 117411. https://doi.org/10.1016/J.EPSL.2022.117411.

van Keken, P.E., Hacker, B.R., Syracuse, E.M., Abers, G.A., 2011. Subduction factory: 4. Depth-dependent flux of H $_2$ O from subducting slabs worldwide. J. Geophys. Res. 116, B01401. https://doi.org/10.1029/2010JB007922.

van Keken, P.E., Wada, I., Abers, G.A., Hacker, B.R., Wang, K., 2018. Mafic high-pressure rocks are preferentially exhumed from warm subduction settings. Geochem. Geophys. Geosyst. 19, 2934–2961. https://doi.org/10.1029/2018GC007624.

Vengosh, A., Kolodny, Y., Starinsky, A., Chivas, A.R., McCulloch, M.T., 1991. Coprecipitation and isotopic fractionation of boron in modern biogenic carbonates. Geochim. Cosmochim. Acta 55, 2901–2910. https://doi.org/10.1016/0016-7037(91)90455-E.

Wada, I., Wang, K., 2009. Common depth of slab-mantle decoupling: reconciling diversity and uniformity of subduction zones. Geochem. Geophys. Geosyst. 10, Q10009. https://doi.org/10.1029/2009GC002570.

Wada, I., Behn, M.D., Shaw, A.M., 2012. Effects of heterogeneous hydration in the incoming plate, slab rehydration, and mantle wedge hydration on slab-derived H 2 O flux in subduction zones. Earth Planet. Sci. Lett. 353–354, 60–71. https://doi.org/10.1016/j.epsl.2012.07.025.

Walker, J.A., Williams, S.N., Kalamarides, R.I., Feigenson, M.D., 1993. Shallow open-system evolution of basaltic magma beneath a subduction zone volcano: The Masaya Caldera Complex, Nicaragua. J. Volcanol. Geotherm. Res. 56, 379–400. https://doi.org/10.1016/0377-0273(93)90004-B.

Walowski, K.J., Wallace, P.J., Clynne, M.A., Rasmussen, D.J., Weis, D., 2016. Slab melting and magma formation beneath the southern Cascade arc. Earth Planet. Sci. Lett. 446, 100–112. https://doi.org/10.1016/J.EPSL.2016.03.044.

Walowski, K.J., Kirstein, L.A., De Hoog, J.C.M., Elliott, T.R., Savov, I.P., Jones, R.E., 2019. Investigating ocean island mantle source heterogeneity with boron isotopes in melt inclusions. Earth Planet. Sci. Lett. 508, 97–108. https://doi.org/10.1016/j.epsl.2018.12.005.

Wieser, P.E., Turner, S.J., Mather, T.A., Pyle, D.M., Savov, I.P., Orozco, G., 2019. New constraints from Central Chile on the origins of enriched continental compositions in thick-crusted arc magmas. Geochim. Cosmochim. Acta 267, 51–74. https://doi.org/10.1016/j.gca.2019.09.008.

Wilson, C.R., Spiegelman, M., van Keken, P.E., Hacker, B.R., 2014. Fluid flow in subduction zones: the role of solid rheology and compaction pressure. Earth Planet. Sci. Lett. 401, 261–274. https://doi.org/10.1016/j.epsl.2014.05.052.

Wunder, B., Meixner, A., Romer, R., Wirth, R., Heinrich, W., 2005. The geochemical cycle of boron: constraints from boron isotope partitioning experiments between mica and fluid. Lithos 84, 206–216. https://doi.org/10.1016/j.lithos.2005.02.003.

Zhang, Y., Gazel, E., Gaetani, G.A., Klein, F., 2021. Serpentinite-derived slab fluids control the oxidation state of the subarc mantle. Sci. Adv. 7, eabj2515. https://doi.org/10.1126/sciadv.abj2515.

Zurek, J., Moune, S., Williams-Jones, G., Vigouroux, N., Gauthier, P.J., 2019. Melt inclusion evidence for long term steady-state volcanism at Las Sierras-Masaya volcano, Nicaragua. J. Volcanol. Geotherm. Res. 378, 16–28. https://doi.org/10.1016/J.JVOLGEORES.2019.04.007.